Journal of RADIATION INDUSTRY
Vol. 19, No. 4, pp. 403-413, 2025
https://doi.org/10.23042/radin.2025.19.4.403

Original article

Assessing DNA Damage in Reduced-Scale Fractal Geometries with Geant4-DNA

Tu Minh Khuong[1,2], Jong-Hyun Jung[1], and Sangyong Lim[1,2,*]

[1]Radiation Biotechnology Division, Korea Atomic Energy Research Institute, Jeongeup 56212, Republic of Korea
[2]Department of Radiation Science, University of Science and Technology, Daejeon 34113, Republic of Korea

ABSTRACT Accurate modeling of radiation-induced DNA damage is critical for understanding radiobiological effects at the nanometer scale. This study evaluates the feasibility of using reduced-scale fractal chromatin geometries to simulate complex DNA damage in Geant4-DNA, with a focus on non-double-strand-break (non-DSB) clustered lesions. Two ellipsoidal models, minihumanA and minihumanB, were developed to preserve the DNA base-pair density (0.015 bp nm^{-3}) of a whole human fibroblast nucleus while minimizing geometric volume. Monte Carlo simulations were performed using γ-rays, protons, and carbon ions to span a wide LET range. The complexity of clustered lesions increased with both LET and particle type, with heavier ions producing more complex breaks. Across all radiation types, non-DSB lesions accounted for 92-98% of total damage, with increasing LET associated with rising DSB yields and declining SSB frequencies, consistent with both prior simulation studies and experimental observations. Notably, despite differing in size and genomic content (13.2 Mbp for minihumanA and 7.2 Mbp for minihumanB), the predicted damage yields aligned closely with experimental findings, indicating that absolute nuclear dimensions and base pair number have minimal influence when chromatin density is preserved. This suggests that density-preserving geometries capture the essential features of radiation-induced damage formation and provide predictions that more closely reflect experimental observations than models based on randomly distributed DNA segments in prior simulation studies. Non-DSB clustered lesions, predominantly complex single-strand breaks with base damage, were the most abundant clustered damage type, with non-DSB-to-DSB ratios ranging from 4.5 to 14. These findings validate the use of downsized, density-preserving models for efficient and biologically realistic DNA damage simulations and underscore the importance of systematically quantifying non-DSB clusters as potentially mutagenic, yet often underappreciated, radiation-induced lesions.

Key words: Monte Carlo simulation, Geant4-DNA, Fractal geometry, Radiation-induced damage, Non-DSB clusters

1. Introduction

Monte Carlo track structure (MCTS) simulations have become essential for understanding radiation-induced DNA damage at the nanometer scale. Several MCTS codes have been developed and utilized in radiobiological studies. Recently published MCTS codes are Monte Carlo N-Particle 6 (MCNP6), PARTRAC (PARticles TRACks), PENELOPE (Penetration and ENErgy LOss of Positrons and Electrons), and Geant4-DNA (GEometry ANd Tracking 4-DNA) [1-9]. Among these, Geant4-DNA stands out as a powerful and widely used toolkit that models interactions of ionizing radiation with water and DNA at a molecular level. Geant4-DNA is specifically designed to simulate radiation-induced events, focusing on DNA damage mechanisms that emerge from track structure interactions in liquid water down to the eV range [7,9]. Geant4-DNA models the physical, physicochemical, and chemical stages of radiation action, offering detailed DNA-scale geometries for damage prediction [8,10].

A standard method of biologically accurate DNA damage modeling involves using fractal chromatin geometries, which reflect the self-similar, non-linear organization of chromosomal DNA within the cell nucleus. This fractal nature is not a theoretical convenience; it is backed by increasing evidence linking spatial genome organization with gene expression regulation, DNA replication, and chromatin dynamics [11-14]. These mod-

ISSN 1976-2402 **http://www.ksri.kr/**

Copyright© 2025 by Korean Society of Radiation Industry

***Corresponding author:** Sangyong Lim
Tel: +82-63-570-3141, Fax: +82-63-570-3149, E-mail: saylim@kaeri.re.kr

Received 17 August 2025 **Revised** 26 August 2025 **Accepted** 22 October 2025

els represent the spatial distribution of DNA, thereby enhancing our understanding of patterns of genetic expression and the spatial organization of chromatin within the nucleus. Despite improving realism, they come with a severe trade-off: extremely high computational cost [15-17]. Simulations using full-scale or fractal-based chromatin geometries require substantial CPU time and memory resources, making them inefficient or even infeasible for high-throughput or clinical applications.

In this work, we investigate the accuracy and feasibility of using a reduced-scale geometry as a substitute for a full-scale human fibroblast nucleus in Geant4-DNA simulations. Rather than modeling the entire nucleus, we employed a smaller geometry that preserves the local chromatin density and structural complexity of the whole model. The DNA damage classification in this study focuses specifically on complex strand breaks and base damage (BD), which are strongly associated with mutation induction and carcinogenesis [18-20]. These lesions are typically more challenging to repair accurately and are therefore more likely to lead to long-term genomic instability than isolated double-strand breaks (DSBs) [21-23]. This study aims to evaluate the feasibility of using reduced-scale, density-preserving fractal chromatin geometries to assess non-DSB clustered lesions. To the best of our knowledge, this represents one of the first applications of fractal-based nuclear models for investigating non-DSB clusters, providing a framework that bridges prior random-segment approaches with a more biologically realistic chromatin organization.

2. Method

2.1. Irradiation simulation in Geant4-DNA

All simulations were performed using the Geant4-DNA extension of the Geant4 Monte Carlo toolkit, version 11.2. The G4EmDNAPhysics_option4 physics constructor was employed throughout the study. This physics list provides an extensive set of electromagnetic processes, tailored explicitly for water radiolysis and DNA-scale track structure modeling, with optimized thresholds for low-energy electrons, protons, and heavier ions. To investigate the feasibility of reduced-size geometries across a wide range of linear energy transfer (LET) values, three distinct radiation types were simulated: ^{60}Co γ-rays (0.2 keV μm^{-1}), protons (LET values ranging from 5 to 47 keV μm^{-1}), and carbon ions (25.2 keV μm^{-1}). All radiations were simulated using General Particle Source. Particles were generated from a circular planar source with a radius of 900 nm, positioned 3 μm from the target geometry and directed along the negative y-axis toward the target. ^{60}Co γ-rays were modeled using two monoenergetic gamma beams of 1.173 MeV and 1.333 MeV, each contributing 50% of the fluence. The number of incident particles ranged from 3×10^8 to 10^9 particles. For protons, the corresponding energy-LET pairs were as follows: 0.4 MeV (47 keV/μm), 0.6 MeV (36 keV/μm), 0.9 MeV (28 keV/μm), 1.5 MeV (19.5 keV/μm), 2.25 MeV (14.5 keV/μm), and 8.5 MeV (5.2 keV/μm). The number of incident protons ranged from 220 to 3000 particles. Carbon ions were modeled as a monoenergetic 94.55 MeV beam, with number of incident particles ranging from 10 to 100 particles.

To model the physico-chemical processes following the initial ionization events, the G4EmDNAChemistry_option3 chemistry constructor was utilized. This configuration includes a water radiolysis model featuring 15 molecular species and 72 chemical reactions, with predefined diffusion coefficients and reaction rates. The chemistry stage was simulated for a duration of 5 nanoseconds, using the Independent Reaction Time (IRT) approach to account for diffusion-controlled chemical interactions among reactive species in the aqueous phase [24-26].

The simulation configuration employed key parameters consistent with established Geant4-DNA modeling practices [24,25]. The direct interaction radius R_{dir} was set to 3.5 Å, representing the maximum distance within which energy depositions were considered to cause direct damage. Strand break thresholds ranged from 5 to 37.5 eV (E_{min}^{break} to E_{max}^{break}), capturing the energy window for inducing single- and double-strand breaks. The probability of strand break induction by hydroxyl radicals (p_{OH}^{break}) was set to 0.405, and the chemical stage duration (T_{chem}) was limited to 5 ns. To restrict radical diffusion within biologically relevant spatial boundaries, the chemical kill radius (d_{kill}^{chem}) was set to 9 nm.

2.2. Damage classification

Ionizing radiation-induced DNA damage was classified according to damage complexity, following the classification scheme proposed initially by Nikjoo *et al*. and subsequently adopted in other MCTS simulations [27-29]. To determine whether multiple lesions formed part of a damage cluster, a maximum distance of 10 base pairs (bp) was used. Lesions occurring within this distance were considered spatially correlated and part of the same damage site. The classification scheme used in this study is illustrated in Fig. 1 and described in Table 1. Among these, SS-B_{cb} is considered the representative non-DSB cluster type in this study. It captures structurally complex configurations that are not

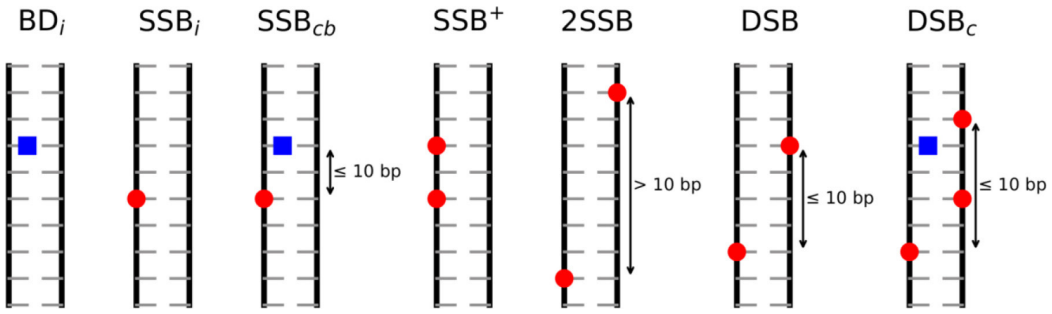

Fig. 1. Schematic representation of DNA damage types classified in this study, adopted from the originally proposed scheme by Nikjoo et al. Red circles indicate strand breaks on the sugar-phosphate backbone, while blue squares represent base damage.

Table 1. DNA damage classification scheme used in this study. The framework is adapted and modified from Nikjoo *et al*. [28]

Damage Type	Definition
BD_i	Isolated base damage occurring without nearby strand breaks (i.e., no other lesions within 10 bp).
SSB_i	Isolated single-strand break on one strand of the DNA helix, with no other lesions within 10 bp.
SSB^+	Two SSBs on the same strand within 10 bp of each other.
2SSB	Two SSBs on opposite strands, separated by more than 10 bp.
SSB_c	Complex SSB, defined as the sum of SSB^+ and 2SSB events (with or without BD).
SSB_{cb}	Non-DSB clustered damage, defined as a cluster containing at least one SSB (SSB_i or SSB_c) and at least one BD within 10 bp.
SSB_{tot}	Total SSBs, defined as the sum of SSB_i, SSB^+, 2SSB, and SSB_{cb}.
DSB	Double-strand break formed by two SSBs on opposite strands located within 10 bp.
DSB_c	Complex DSB, defined as a DSB accompanied by at least one additional lesion (SSB or BD) within 10 bp of either strand break.
DSB_{tot}	Total DSBs, defined as the sum of DSB and DSB_c.

classified as DSBs but may be repair-resistant and biologically consequential. In addition, complex base damage involving multiple adjacent BDs was not considered in this study.

2.3. Geometry modifications

Geometrical models in this study were implemented in Geant4-DNA to investigate the induction of DNA damage following exposure to ionizing radiation. The nuclear geometry was generated using the FractalDNA tool [30]. The FractalDNA tool is integrated explicitly with the molecularDNA example of Geant4-DNA, enabling high-resolution simulations of radiation-induced damage within a geometrically and biologically accurate representation of the human genome [25,26]. By leveraging the Hilbert space-filling curve, FractalDNA spatially maps the linear genome into a 3D chromatin architecture. Figure 2 is the simplified illustration of the fractal geometries generated from FractalDNA. A 3D ellipsoidal mask was applied to the structure to achieve the shape of a human fibroblast nucleus.

This fractal structure is then voxelized, with each voxel representing a discrete chromatin segment. This voxel-based implementation allows Geant4-DNA to assign and track individual DNA segments and their chemical components (e.g., sugar-phosphate backbones, bases) within a densely packed, yet biologically faithful, nuclear environment. The result is a comprehensive, nanoscale-resolution geometry from which a structured *dataframe* can be extracted, representing the spatial and molecular configuration of the chromatin. This *dataframe* contains detailed information for each voxel, including its genomic coordinates, bp content, and atomic structure, which are essential for accurate scoring of radiation-induced damage. The extracted *dataframe* serves as a direct input to the Geant4-DNA's "molecularDNA" example. Within this framework, each molecular component, down to individual sugar, phosphate, and base groups, is explicitly placed in 3D space, enabling the simulation to resolve direct damage events at atomic resolution.

To evaluate the feasibility of reduced-scale geometries for DNA damage prediction, two downsized models, minihumanA and minihumanB, were constructed. These models were derived by scaling down the dimensions of a whole human fibroblast nucleus, based on the geometry described by Chatzipapas *et al*.

[25]. The whole human nucleus model represents a fibroblast nucleus with dimensions of 7100 × 2500 × 7100 nm semi-axes and approximately 6.4 Gbp of genomic content, corresponding to a DNA packing density of approximately 0.015 bp nm^{-3}. MinihumanA was designed as an ellipsoid with axes 900 × 317 × 900 nm semi-axes and contains approximately 13.2 Mbp of DNA. MinihumanB, with a distinguished dimensional ratio of 900 × 400 × 400 nm semi-axes, includes roughly 7.2 Mbp. Both models were generated to match the DNA packing density of the full-scale geometry (approximately 0.015 bp nm^{-3}), ensuring that the local chromatin concentration and folding complexity were preserved, despite the overall volume reduction.

3. Result

Figures 3 and 4 present the composition of radiation-induced DNA damage in terms of SSB_{tot}, DSB_{tot}, and BD for γ-rays, carbon ions, and protons. Across all radiation types, BD_i consistently accounts for approximately 40-48% of the total lesion count. SSB_{tot} comprises 40-58%, while DSB_{tot} increases with LET and contributes up to approximately 9% for carbon ion exposure. Hence, non-DSB lesions constitute approximately 92-98% of all DNA damage events. A key observation is the shift in damage composition with increasing LET: as LET rises, DSB_{tot} increases markedly, while SSB_{tot} declines. This general trend is consistent

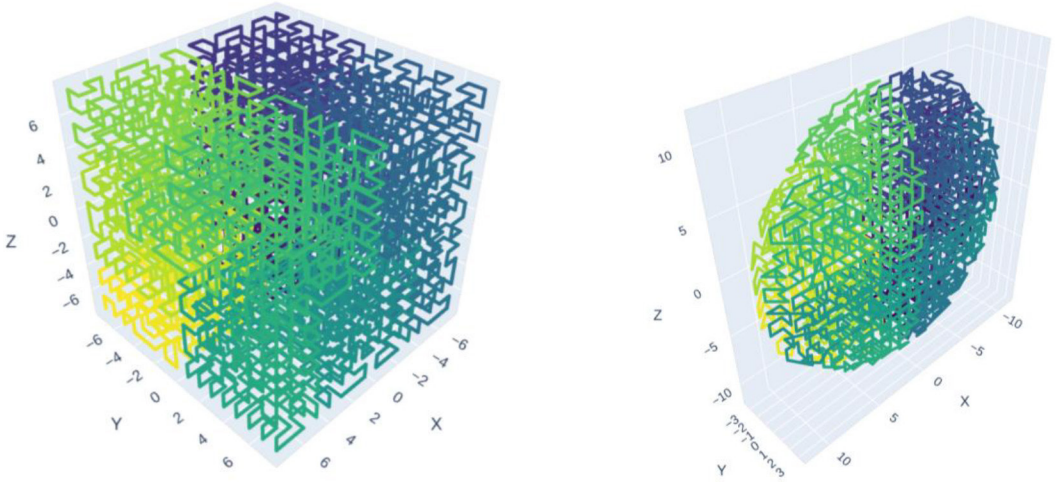

Fig. 2. Simplified fractal geometries generated by FractalDNA, before (left) and after (right) applying an ellipsoidal mask.

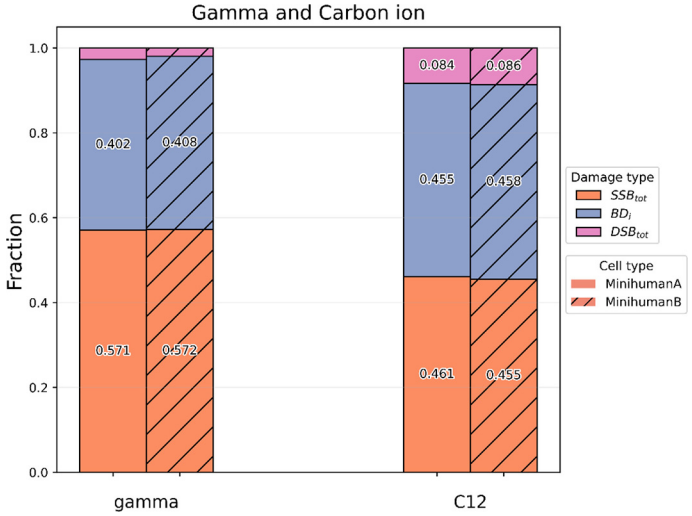

Fig. 3. Fractional distribution of complex DNA damage types (SSB_{tot}, BD_i, DSB_{tot}), induced by γ and carbon ion irradiation across different LET values for two cell models (MinihumanA and minihumanB).

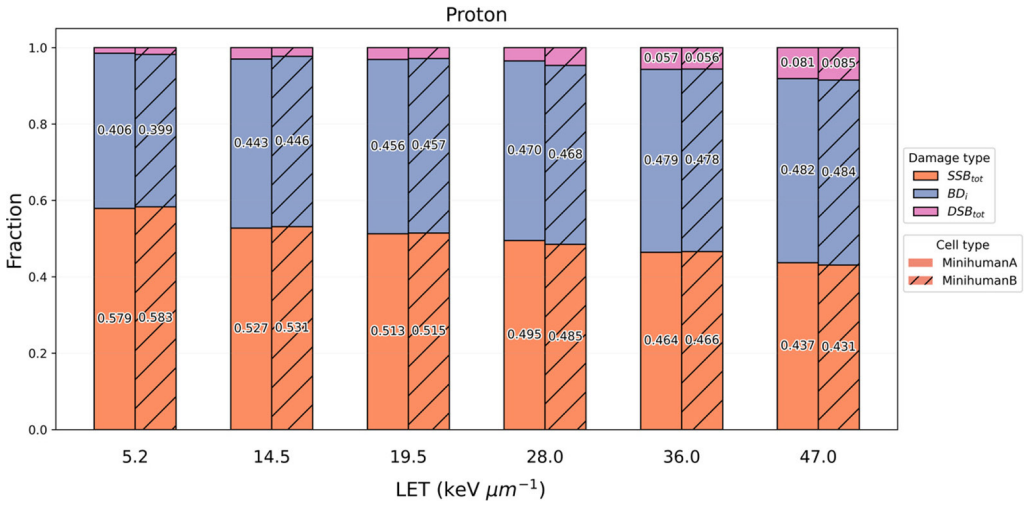

Fig. 4. Fractional distribution of complex DNA damage types (SSB_{tot}, BD_i, DSB_{tot}), induced by proton irradiation across different LET values for two cell models (MinihumanA and minihumanB).

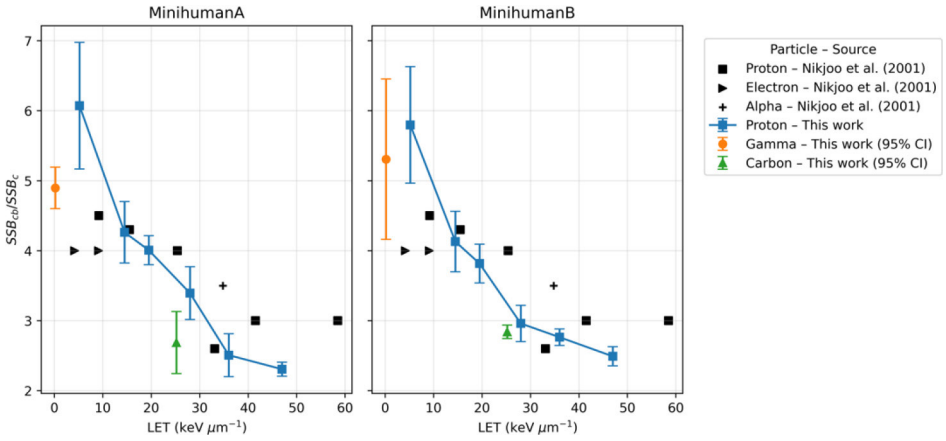

Fig. 5. Ratio of SSB_{cb} to SSB_c as a function of LET for minihumanA and minihumanB cells irradiated with proton, γ, and carbon ion beams, compared to experimental data from Nikjoo et al. [28]. Error bars represent 95% confidence intervals of the mean for all particles.

with previous MCTS simulation studies. MCTS simulation studies by Nikjoo *et al*. [28] and Watanabe *et al*. [29] have shown that non-DSB damage accounted for nearly 99% of all DNA damage at low LET, and still dominate at high LET, comprising approximately 85% of total damage even at LET values as high as 165 keV μm^{-1} (e.g., Fe ions).

Figure 5 highlights the LET dependence of complex SSB by showing the ratio of SSB_{cb}/SSB_c. γ and low-LET proton irradiation cases show high SSB_{cb}/SSB_c ratios, around 6.0 to 5. A clear inverse relationship is observed between LET and the SSB_{cb}/SSB_c ratio across all proton irradiation cases. For carbon ion exposure at 25.2 keV μm^{-1}, both minihumanA and minihumanB models yield a SSB_{cb}/SSB_c ratio of approximately 2.7. The predictions are broadly consistent with prior simulations from Nikjoo *et al*. [28]. However, our configurations resulted in a lower SSB_{cb}/SSB_c ratio at higher LET due to the difference in geometries used. Nikjoo's simulations modeled linear B-DNA segments randomly distributed as chords within a cylindrical volume, a configuration that effectively increases local DNA accessibility to ion tracks. By contrast, the density-preserving fractal chromatin geometries used in minihumanA and minihumanB incorporate chromatin compaction and continuity, thereby reducing apparent DNA overexposure and yielding more conservative estimates of complex SSB formation.

This trend is further explained by the breakdown in Fig. 6, where the decline in SSB_{tot} (Figs. 3 and 4) is shown to be driven primarily by a reduction in both SSB_i and SSB_{cb}. Although it is expected that DSB_{tot} yield increases with LET due to greater

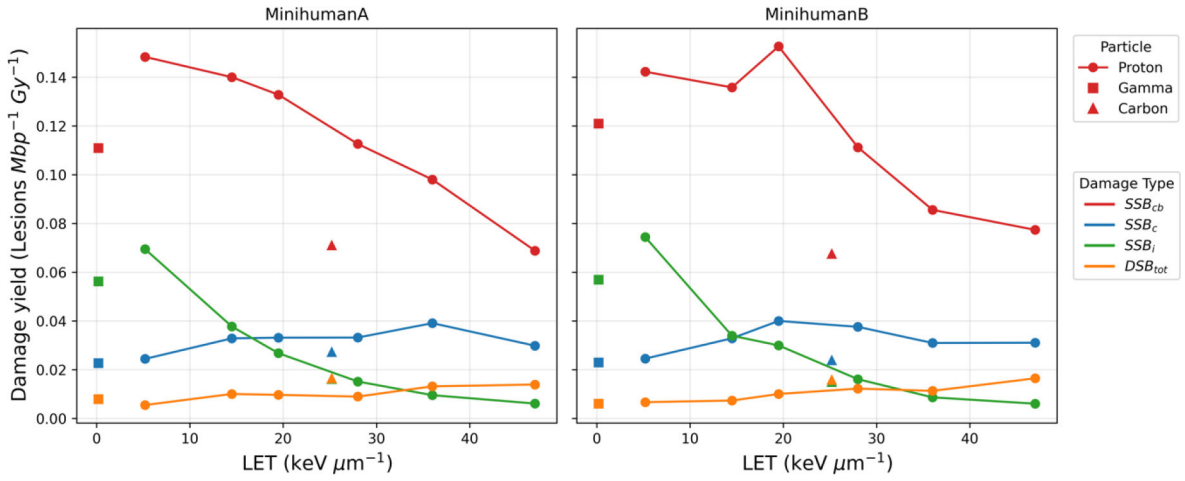

Fig. 6. Yields of DSB_{tot} and SSB-relevant DNA damage types as a function of LET across different radiation types and cell models. Proton, γ-ray, and carbon ion results are represented by closed circles, closed squares, and closed triangles, respectively.

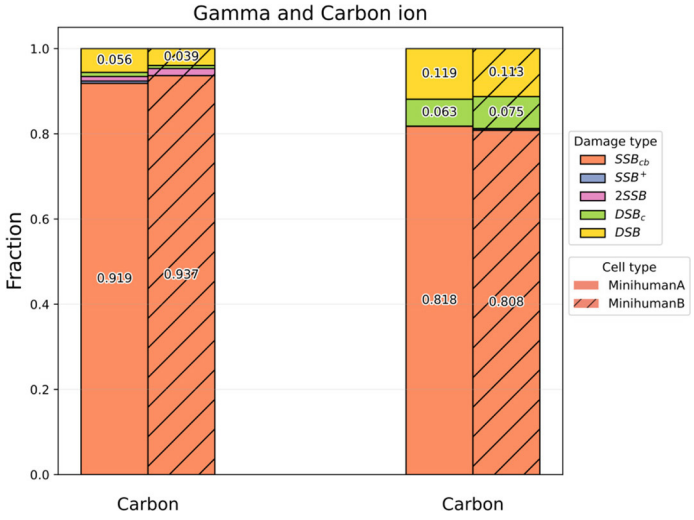

Fig. 7. Fractional distribution of complex DNA damage types, induced by γ and carbon ion irradiation for two cell models (MinihumanA and minihumanB).

energy deposition density, it is worth noting that non-DSB damage remains dominant even at high LET. At 47 keV μm^{-1} proton exposure, the yield of SSB_{cb} is approximately five times higher than that of DSB_{tot}. Similarly, for carbon ions at 25.2 keV μm^{-1}, the SSB_{cb} to DSB_{tot} ratio remains high, averaging 4.5 for both minihumanA and minihumanB.

In the context of clustered lesions, non-DSB clustered damage, SSB_{cb}, remains the primary component of total DNA damage, even under high-LET conditions. Specifically, SSB_{cb} alone accounts for approximately 81-95% of the total clustered lesion yield across conditions studied, underscoring the continued dominance of non-DSB clusters in the overall damage landscape (Figs. 7 and 8). Additionally, the proportion of DSB_c increases not only with LET but also with the nature of the radiation source. For heavier ions such as carbon, the complexity of DSBs is more pronounced compared to protons, even at similar or higher LET values.

Despite the reduced size and base-pair content of the minihumanA and minihumanB geometries compared to a full-scale cell nucleus, their density-preserving fractal models yielded results that align more closely with experimental observations than previous random-segment or full-volume models. The preserved chromatin density and structural organization in both minihuman geometries ensured realistic spatial correlations, yielding biologically plausible damage distributions across all radiation types. This contrasts with earlier modeling approaches that used

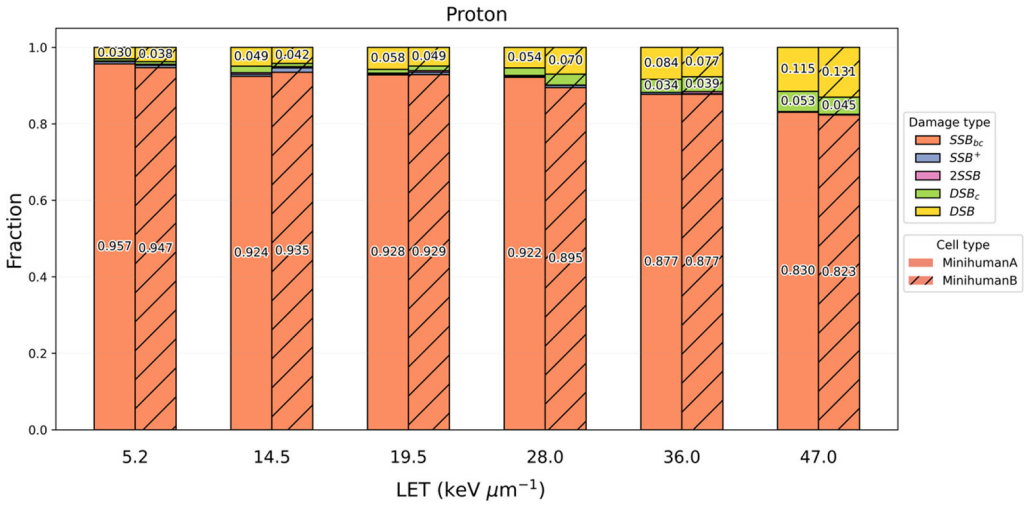

Fig. 8. Fractional distribution of complex DNA damage types, induced by proton irradiation for two cell models (MinihumanA and minihumanB).

randomly distributed B-DNA segments, which typically exhibited greater accessibility to ionizing tracks, resulting in higher damage yields [31].

4. Discussion

Previous studies have primarily focused on DNA strand breaks, particularly SSBs, DSBs, and DSB_c complex clusters, due to their established roles in cellular outcomes such as repair and lethality [24,25,28,29,31-33]. Although DSBs are classically associated with cytotoxicity and are considered the primary lesions leading to cell death, studies have shown that clustered non-DSB damage, particularly involving oxidized base lesions, is also highly repair-resistant and biologically consequential [18,34-36]. Such lesions can interfere with DNA processing and, if not properly resolved, may convert into DSBs during repair attempts [22,23,37]. The misrepaired damage contributes to increased mutational burden and genomic instability [38,39]. Moreover, high-LET radiation has been associated with a greater complexity of non-DSB lesions and a higher frequency of their erroneous repair, leading to an elevated risk of mutation compared to low-LET exposures [37].

Increasing evidence suggests that non-DSB clustered lesions are not only more abundant than DSBs but may also be critical contributors to radiation-induced DNA damage [28,29,32,40-43]. Sahbani *et al*. [44] demonstrated that non-DSB clusters are responsible for the loss of plasmid DNA functionality in the presence of cisplatin, with their yield exceeding that of DSBs by a factor of 26. Our results fall between simulation predictions and experimental findings [28,29,32,40], reinforcing the prevalence of non-DSB clustered lesions (Figs. 3 and 4). As shown in Figs. 7 and 8, the dominance of SSB_{cb} over DSB and DSB_c yields across all particle types underscores the importance of systematically evaluating non-DSB clustered lesions, which may be underappreciated contributors to radiation-induced mutagenesis.

Experimental data also consistently show that the ratio of non-DSB clustered lesions to DSBs ranges from 3 to 8, and non-DSB clusters were estimated to constitute 50-80% of all complex lesions at elevated LETs [41-43]. In comparison, our simulation results yield a higher non-DSB-to-DSB ratio, ranging from 4.5 to 14 across different radiation types and LET values. Notably, even under high-LET conditions, non-DSB clusters, particularly SSB_{cb}, continue to outnumber DSBs. In the case of carbon ion exposure at 25.2 keV μm^{-1} (Fig. 7), non-DSB clustered lesions account for approximately 82% of total clustered damage, based on the average of minihumanA and minihumanB results.

While the biological significance and repair challenges of non-DSB clustered lesions are increasingly recognized [37,39], the quantification of such damage varies widely across different experimental and simulation configurations. Numerous studies, both computational and experimental, have employed diverse biological models, including human fibroblasts, monocytes, hamster V79-4 lung fibroblasts, and plasmid DNA, each yielding different absolute values of cluster damage [22,28,41,42,45,46]. For instance, in the case of γ-ray exposure, reported yields of oxidative base lesions such as 8-Oxo-7,8-dihydro-2'-deoxyguanosine (8-oxodG) in human fibroblasts are approximately 0.0095

lesions 10^{-6} bases Gy^{-1}, while in THP-1 monocyte cells, values range from 0.011 to 0.020 lesions 10^{-6} bases Gy^{-1} [45,47,48]. These variations are not only due to differences in DNA sequence or repair capacity but also reflect the structural and spatial characteristics of DNA packing within the models [49-51].

Previous studies have explored the relationship between DNA structure and damage yield, showing that a compact geometry registered a greater number of particle interactions per track compared to a more relaxed one [52,53]. However, when damage yields are normalized by the number of bp, relaxed geometries consistently exhibit higher damage rates per unit DNA, highlighting an inverse relationship between chromatin compactness and lesion frequency. Meylan *et al*. [52] explicitly demonstrated this effect, showing that DNA compactness plays a critical role in modulating strand break induction by comparing damage yields in extended versus condensed DNA geometries.

This finding is supported by other simulation studies suggesting that chromatin compaction, rather than nuclear shape or size, is the dominant factor in determining the yield and complexity of DNA damage [31,54,55]. Lampe *et al*. [31] used *Escherichia coli* (*E. coli*) geometry as a surrogate for human chromatin and demonstrated that DNA damage yields should not be strongly dependent on overall geometry, particularly employing continuous, biologically realistic DNA structures. Their findings support the notion that DNA density and continuity of the DNA strand play a more critical role in damage prediction than the absolute shape or size of the geometry. Denser chromatin structures, while absorbing more energy per unit volume, tend to produce fewer lesions per bp, suggesting a protective effect conferred by DNA packaging [56].

Our study investigates this concept further by employing two scaled-down minihuman geometries that maintain identical base-pair densities but differ in overall shape and size. This approach allows us to isolate the influence of geometry versus density in determining DNA damage yields, and to assess whether absolute cell dimensions meaningfully affect the spatial distribution of radiation-induced lesions when chromatin density is preserved. The results from our simulations indicate a lower non-DSB cluster yield compared to previous simulation data. Earlier studies using B-DNA segments randomly distributed within a defined water volume may make the target DNA more exposed to particle hits, leading to an overestimation of damage yields by neglecting spatial constraints and biological DNA compaction [28,29,32]. In contrast, our use of structured, density-preserved chromatin geometries introduces more realistic spatial correlations, resulting in more conservative and biologically plausible estimates of complex lesion formation. Importantly, the damage yields obtained from both minihumanA and minihumanB geometries align more closely with experimental observations across all radiation types, suggesting that density-preserving fractal packing provides a more accurate representation of DNA damage formation than previous random-segment approaches [28,29,32]. This finding supports the scalability of reduced-volume models and offers a significant practical advantage: smaller geometries reduce computational cost and simulation time without sacrificing biological fidelity. Despite the higher frequency of non-DSB clusters relative to DSBs is expected, our simulations provide novel quantitative insights into the non-DSB-toDSB ratios across multiple radiation types and LET values. We demonstrate that the dominance of non-DSB clusters is robust across different radiation types, highlighting both the biological relevance of SSB_{cb} lesions and the practical utility of compact geometries for efficient and realistic DNA damage modeling.

We acknowledge that the current fractal-based structure in this study does not fully capture the complexity of the human nucleus, but the use of density-preserving fractal chromatin geometries provides a more biologically plausible framework than earlier random-segment approaches. By incorporating realistic chromatin packing and spatial correlations, the model approximates non-DSB cluster yields that align well with experimental observations, suggesting that key features of radiation-induced DNA damage can be meaningfully captured even in reduced-scale simulations. Future work integrating experimental measurements could further refine these predictions and enhance their biological fidelity.

Moreover, the use of smaller-volume geometries becomes especially relevant when moving toward multicellular or tissue-scale modeling, where current single-cell simulations often neglect intercellular gaps and extracellular spacing. These structural voids, present in realistic cell cultures or tissue environments, would reduce the effective target density and consequently lower damage yields in actual experiments [57]. Without accounting for these spatial effects, full-volume single-cell models may overestimate biological impact while consuming disproportionately high computational resources [25, 28, 58-60]. Employing compact, density-matched sub-cellular geometries offers a viable path to bridge this gap between idealized simulations and realistic biological scenarios.

While the results from this study place specific emphasis on the abundance of non-DSB clustered damage, it is also import-

ant to acknowledge that our current classification of non-DSB clusters is limited to SSB_{cb}. This aggregated classification is a necessary simplification, but it represents only the first step in quantifying biologically relevant non-DSB lesions. The repair pathways for non-DSB clusters are highly context-dependent, and specific lesion types invoke distinct enzymatic responses. For example, clusters containing 8-oxodG are typically processed via OGG1-mediated base excision repair, whereas thymine glycol lesions are handled by endonuclease III (Nth) [18]. Therefore, future work should aim to move beyond damage yield quantification by implementing complex BD scoring and clustering, which will allow for more mechanistic modeling of repair outcomes. Incorporating lesion-type resolution into MCTS simulations would significantly enhance the biological fidelity of predictions and provide deeper insight into mutation risk, repair efficiency, and radiosensitization strategies.

5. Conclusion

To assess the impact of DNA density and evaluate the feasibility of scaling genomic geometries, we employed a reduced-scale geometry representing a smaller segment of the cell nucleus. This approach was designed to test the hypothesis that absolute cell size is not a critical factor for predicting direct DNA damage, provided that the local chromatin density is preserved. By maintaining equivalent DNA packing density and structural complexity in the scaled-down model, we demonstrated that accurate damage prediction could be achieved without simulating an entire nucleus. This finding supports the potential for computationally efficient, modular modeling of multicellular systems, where biologically relevant damage outcomes can be retained even with simplified or partitioned geometries.

Moreover, by focusing on SSB_{cb}, which is highly prevalent, repair-resistant, and biologically consequential, we highlighted the importance of modeling lesion types beyond traditional strand breaks. Our results confirmed that SSB_{cb} remains dominant even at high LET. While this study quantified clustered damage in aggregate form, future work will aim to resolve individual base lesion types within clusters, enabling more precise modeling of repair dynamics, enzymatic processing, and mutagenic potential. This progression will be critical for advancing nanoscale radiation biology toward more predictive, mechanism-based applications in radiotherapy, space biology, and radiological protection.

Acknowledgement

This research was supported by the KAERI Institutional R&D program (project No. 523610-25).

References

1. Goorley T, James M, Booth T, Brown F, Bull J, Cox LJ, Durkee, J, Elson, J, Fensin M, Forster RA, Hendricks J, Hughes HG, Johns R, Kiedrowski B, Martz R, Mashnik S, McKinney G, Pelowitz D, Prael R and Zukaitis T. 2014. Features of mcnp6. *SNA+MC 2013 – Joint International Conference on Supercomputing in Nuclear Applications+Monte Carlo*, 06011. https://doi.org/10.1051/snamc/201406011.
2. Fernández-Varea JM, González-Muñoz G, Galassi ME, Wiklund K, Lind BK, Ahnesjö A and Tilly N. 2012. Limitations (And merits) of PENELOPE as a track-structure code. *Int. J. Radiat. Biol.* **88**(1-2):66-70. https://doi.org/10.3109/09553002.2011.598209.
3. Bäckström G, Galassi ME, Tilly N, Ahnesjö A and Fernández-Varea JM. 2013. Track structure of protons and other light ions in liquid water: Applications of the LIonTrack code at the nanometer scale. *Med. Phys.* **40**(6Part1):064101. https://doi.org/10.1118/1.4803464.
4. Villegas F, Tilly N and Ahnesjö A. 2013. Monte Carlo calculated microdosimetric spread for cell nucleus-sized targets exposed to brachytherapy125 I and192 Ir sources and60 Co cell irradiation. *Phys. Med. Biol.* **58**(17):6149-6162. https://doi.org/10.1088/0031-9155/58/17/6149.
5. Nikjoo H, Uehara S, Emfietzoglou D and Cucinotta FA. 2006. Track-structure codes in *Radiat. Res. Radiat. Meas.* **41**(9):1052-1074. https://doi.org/10.1016/j.radmeas.2006.02.001.
6. Friedland W, Jacob P, Paretzke HG, Merzagora M and Ottolenghi A. 1999. Simulation of DNA fragment distributions after irradiation with photons. *Radiat. Environ. Biophys.* **38**(1):39-47. https://doi.org/10.1007/s004110050136.
7. Incerti S, Baldacchino G, Bernal M, Capra R, Champion C, Francis Z, Guèye P, Mantero A, Mascialino B, Moretto P, Nieminen P, Villagrasa C and Zacharatou C. 2010. The geant4-dna project. *Int. J. Model. Simul. Sci. Comput.* **01**(02):157-178. https://doi.org/10.1142/S1793962310000122.
8. Incerti S, Kyriakou I, Bernal MA, Bordage MC, Francis Z, Guatelli S, Ivanchenko V, Karamitros M, Lampe N, Lee SB, Meylan S, Min CH, Shin WG, Nieminen P, Sakata D, Tang N, Villagrasa C, Tran HN and Brown JMC. 2018. Geant4-DNA example applications for track structure simulations in liquid water: A report from the Geant4-DNA Project. *Med. Phys.* **45**(8). https://doi.org/10.1002/mp.13048.
9. Bernal MA, Bordage MC, Brown JMC, Davídková M, Delage E, El Bitar Z, Enger SA, Francis Z, Guatelli S, Ivanchenko VN, Karamitros M, Kyriakou I, Maigne L, Meylan S, Murakami K, Okada S, Payno H, Perrot Y, Petrovic I, Incerti S. 2015. Track structure modeling in liquid water: A review of the Geant4-DNA very low energy extension of the Geant4 Monte Carlo simulation toolkit. *Phys. Med.* **31**(8):861-874. https://doi.org/10.1016/j.ejmp.2015.10.087.

10. Kyriakou I, Sakata D, Tran HN, Perrot Y, Shin WG, Lampe N, Zein S, Bordage MC, Guatelli S, Villagrasa C, Emfietzoglou D and Incerti S. 2021. Review of the geant4-dna simulation toolkit for radiobiological applications at the cellular and dna level. *Cancers*, **14**(1):35. https://doi.org/10.3390/cancers14010035.
11. Correia JP, Silva R, Anselmo DHAL, Vasconcelos MS and Da Silva LR. 2024. Multifractal properties of human chromosome sequences. *Fractal Fract.* **8**(6):312. https://doi.org/10.3390/fractalfract8060312.
12. Lee SH, Kim Y, Lee S, Durang X, Stenberg P, Jeon JH and Lizana L. 2019. Mapping the spectrum of 3D communities in human chromosome conformation capture data. *Sci. Rep.* **9**(1):6859. https://doi.org/10.1038/s41598-019-42212-y.
13. Lieberman-Aiden E, Van Berkum NL, Williams L, Imakaev M, Ragoczy T, Telling A, Amit I, Lajoie BR, Sabo PJ, Dorschner MO, Sandstrom R, Bernstein B, Bender MA, Groudine M, Gnirke A, Stamatoyannopoulos J, Mirny LA, Lander ES and Dekker J. 2009. Comprehensive mapping of long-range interactions reveals folding principles of the human genome. *Science*, **326**(5950):289-293. https://doi.org/10.1126/science.1181369.
14. Mirny LA. 2011. The fractal globule as a model of chromatin architecture in the cell. *Chromosome Res.* **19**(1):37-51. https://doi.org/10.1007/s10577-010-9177-0.
15. D-Kondo N, Moreno-Barbosa E, Štěphán V, Stefanová K, Perrot Y, Villagrasa C, Incerti S, De Celis Alonso B, Schuemann J, Faddegon B and Ramos-Méndez J. 2021. DNA damage modeled with Geant4-DNA: Effects of plasmid DNA conformation and experimental conditions. *Phys. Med. Biol.* **66**(24):245017. https://doi.org/10.1088/1361-6560/ac3a22.
16. Le TA, Tran NH, Thibaut Y, Chatzipapas K, Sakata D, Incerti S, Villagrasa C and Perrot Y. 2024. "Dsbandrepair" – an updated geant4-dna simulation tool for evaluating the radiation-induced dna damage and its repair. *Phys. Med.* **124**:103422. https://doi.org/10.1016/j.ejmp.2024.103422.
17. Tian Z, Jiang SB and Jia X. 2017. Accelerated Monte Carlo simulation on the chemical stage in water radiolysis using GPU. *Phys. Med. Biol.* **62**(8):3081-3096. https://doi.org/10.1088/1361-6560/aa6246.
18. Cadet J, Bourdat AG, D'Ham C, Duarte V, Gasparutto D, Romieu A and Ravanat JL. 2000. Oxidative base damage to DNA: Specificity of base excision repair enzymes. *Mutat.Res. Rev. Mutat. Res.* **462**(2):121-128. https://doi.org/10.1016/S1383-5742(00)00022-3.
19. Nickoloff JA, Sharma N and Taylor L. 2020. Clustered dna double-strand breaks: Biological effects and relevance to cancer radiotherapy. *Genes*, **11**(1):99. https://doi.org/10.3390/genes11010099.
20. Rezaee M and Adhikary A. 2024. The effects of particle let and fluence on the complexity and frequency of clustered dna damage. *DNA*, **4**(1):34-51. https://doi.org/10.3390/dna4010002.
21. David-Cordonnier MH, Cunniffe SMT. Hickson ID and O'Neill P. 2002. Efficiency of incision of an ap site within clustered dna damage by the major human ap endonuclease. *Biochemistry*, **41**(2):634-642. https://doi.org/10.1021/bi011682l.
22. Gulston M. 2004. Processing of clustered DNA damage generates additional double-strand breaks in mammalian cells post-irradiation. *Nucleic Acids Res.* **32**(4):1602-1609. https://doi.org/10.1093/nar/gkh306.
23. Eccles LJ, Lomax ME and O'Neill P. 2010. Hierarchy of lesion processing governs the repair, double-strand break formation and mutability of three-lesion clustered DNA damage. *Nucleic Acids Res.* **38**(4):1123-1134. https://doi.org/10.1093/nar/gkp1070.
24. Sakata D, Lampe N, Karamitros M, Kyriakou I, Belov O, Bernal MA, Bolst D, Bordage MC, Breton V, Brown JMC, Francis Z, Ivanchenko V, Meylan S, Murakami, K. Okada S, Petrovic I, Ristic-Fira A, Santin G, Sarramia D, Incerti S. 2019. Evaluation of early radiation DNA damage in a fractal cell nucleus model using Geant4-DNA. *Phys. Med.* **62**:152-157. https://doi.org/10.1016/j.ejmp.2019.04.010.
25. Chatzipapas KP, Tran NH, Dordevic M, Zivkovic S, Zein S, Shin W, Sakata D, Lampe N, Brown JMC, Ristic-Fira A, Petrovic I, Kyriakou I, Emfietzoglou D, Guatelli S and Incerti S. 2023. Simulation of DNA damage using Geant4-DNA: An overview of the "molecularDNA" example application. *Precis. Radiat. Oncol.* **7**(1):4-14. https://doi.org/10.1002/pro6.1186.
26. Chatzipapas K, Dordevic M, Zivkovic S, Tran NH, Lampe N, Sakata D, Petrovic I, Ristic-Fira A, Shin WG, Zein S, Brown JMC, Kyriakou I, Emfietzoglou D, Guatelli S and Incerti S. 2023. Geant4-DNA simulation of human cancer cells irradiation with helium ion beams. *Phys. Med.* **112**:102613. https://doi.org/10.1016/j.ejmp.2023.102613.
27. Nikjoo H, O'Neill P, Terrissol M and Goodhead DT. 1999. Quantitative modelling of DNA damage using Monte Carlo track structure method. *Radiat. Environ. Biophys*, **38**(1):31-38. https://doi.org/10.1007/s004110050135.
28. Nikjoo H, O'Neill P, Wilson WE and Goodhead DT. 2001. Computational approach for determining the spectrum of dna damage induced by ionizing radiation. *Radiat. Res.* **156**(5):577-583. https://doi.org/10.1667/0033-7587(2001)156[0577:cafdts]2.0.co;2.
29. Watanabe R, Rahmanian S and Nikjoo H. 2015. Spectrum of radiation-induced clustered non-dsb damage – a monte carlo track structure modeling and calculations. *Radiat. Res.* **183**(5):525-540. https://doi.org/10.1667/RR13902.1.
30. Lampe N. 2021. Fractaldna [Python]. https://github.com/natl/fractaldna (Original work published 2016).
31. Lampe N, Karamitros M, Breton V, Brown JMC, Sakata D, Sarramia D and Incerti. 2018. Mechanistic DNA damage simulations in Geant4-DNA Part 2: Electron and proton damage in a bacterial cell. *Phys. Med.* **48**:146-155. https://doi.org/10.1016/j.ejmp.2017.12.008.
32. Matsuya Y, Nakano T, Kai T, Shikazono N, Akamatsu K, Yoshii Y and Sato T. 2020. A simplified cluster analysis of electron track structure for estimating complex dna damage yields. *Int. J. Mol. Sci.* **21**(5):1701. https://doi.org/10.3390/ijms21051701.
33. Meylan S, Incerti S, Karamitros M, Tang N, Bueno M, Clairand I and Villagrasa C. 2017. Simulation of early DNA damage after the irradiation of a fibroblast cell nucleus using Geant4-DNA. *Sci. Rep*. **7**(1):11923. https://doi.org/10.1038/s41598-017-11851-4.
34. Nikitaki Z, Nikolov V, Mavragani IV, Mladenov E, Mangelis A, Laskaratou DA, Fragkoulis GI, Hellweg CE, Martin OA, Emfietzoglou D, Hatzi VI, Terzoudi GI, Iliakis G and Georgakilas AG. 2016. Measurement of complex DNA damage induction and repair in human cellular systems after exposure to ionizing radiations of varying linear energy transfer (Let). *Free Radic. Res.* **50**(sup1):S64-S78. https://doi.org/10.1080/10715762.2016.1232484.
35. Goodhead DT. 1994. Initial events in the cellular effects of ionizing radiations: Clustered damage in dna. *Int. J. Radiat. Biol.* **65**(1):7-17. https://doi.org/10.1080/09553009414550021.
36. Dianov GL, O'Neill P and Goodhead DT. 2001. Securing genome stability by orchestrating DNA repair: Removal of radiation-in-

duced clustered lesions in DNA. *BioEssays* **23**(8):745-749. https://doi.org/10.1002/bies.1104.
37. Eccles LJ, O'Neill P and Lomax ME. 2011. Delayed repair of radiation induced clustered DNA damage: Friend or foe? *Mutat Res. Fundamental and Molecular Mechanisms of Mutagenesis*, **711**(1-2):134-141. https://doi.org/10.1016/j.mrfmmm.2010.11.003.
38. Mouw KW, Goldberg MS, Konstantinopoulos PA and D'Andrea AD. 2017. Dna damage and repair biomarkers of immunotherapy response. *Cancer Discov.* **7**(7):675-693. https://doi.org/10.1158/2159-8290.CD-17-0226.
39. Németh E and Szüts D. 2024. The mutagenic consequences of defective DNA repair. *DNA Repair*, **139**:103694. https://doi.org/10.1016/j.dnarep.2024.103694.
40. Xu X, Nakano T, Tsuda M, Kanamoto R, Hirayama R, Uzawa A and Ide H. 2020. Direct observation of damage clustering in irradiated DNA with atomic force microscopy. *Nucleic Acids Res.* **48**(3):e18-e18. https://doi.org/10.1093/nar/gkz1159.
41. Sutherland BM, Bennett PV, Sidorkina O and Laval J. 2000. Clustered DNA damages induced in isolated DNA and in human cells by low doses of ionizing radiation. *PNAS* **97**(1):103-108. https://doi.org/10.1073/pnas.97.1.103.
42. Sutherland BM, Bennett PV, Sutherland JC and Laval J. 2002. Clustered dna damages induced by x rays in human cells. *Radiat. Res*. **157**(6):611-616. https://doi.org/10.1667/0033-7587(2002)157%5B0611:CDDIBX%5D2.0.CO;2.
43. Gulston M. 2002. Clustered DNA damage induced by gamma radiation in human fibroblasts (Hf19), hamster (V79-4) cells and plasmid DNA is revealed as Fpg and Nth sensitive sites. *Nucleic Acids Res.* **30**(15):3464-3472. https://doi.org/10.1093/nar/gkf467.
44. Kouass Sahbani S, Rezaee M, Cloutier P, Sanche L and Hunting DJ. 2014. Non-DSB clustered DNA lesions induced by ionizing radiation are largely responsible for the loss of plasmid DNA functionality in the presence of cisplatin. *Chem.-Biol.Interact.* **217**:9-18. https://doi.org/10.1016/j.cbi.2014.04.004.
45. Jeong HG, Youn CK, Cho HJ, Kim, SH, Kim MH, Kim HB, Chang IY, Lee YS, Chung MH and You HJ. 2004. Metallothionein-iii prevents γ-ray-induced 8-oxoguanine accumulation in normal and hogg1-depleted cells*. *J. Biol. Chem.* **279**(33):34138-34149. https://doi.org/10.1074/jbc.M402530200.
46. Kennedy LJ, Moore K, Caulfield JL, Tannenbaum SR and Dedon PC. 1997. Quantitation of 8-oxoguanine and strand breaks produced by four oxidizing agents. *Chem. Res. Toxicol.* **10**(4):386-392. https://doi.org/10.1021/tx960102w.
47. Pouget JP, Douki T, Richard MJ and Cadet J. 2000. Dna damage induced in cells by γ and uva radiation as measured by hplc/gc−ms and hplc−ec and comet assay. *Chem. Res. Toxicol.* **13**(7):541-549. https://doi.org/10.1021/tx000020e.
48. Pouget JP, Frelon S, Ravanat JL, Testard I, Odin F and Cadet J. 2002. Formation of modified dna bases in cells exposed either to gamma radiation or to high-let particles1. *Radiat. Res.* **157**(5):589-595. https://doi.org/10.1667/0033-7587(2002)157%5B0589:FOMDBI%5D2.0.CO;2.
49. Adeel MM, Rehman K, Zhang Y, Arega Y and Li G. 2022. Chromosomal translocations detection in cancer cells using chromosomal conformation capture data. *Genes* **13**(7):1170. https://doi.org/10.3390/genes13071170.
50. Jin F, Li Y, Dixon JR, Selvaraj S, Ye Z, Lee AY, Yen CA, Schmitt AD, Espinoza CA and Ren B. 2013. A high-resolution map of the three-dimensional chromatin interactome in human cells. *Nature* **503**(7475):290-294. https://doi.org/10.1038/nature12644.
51. Rao SSP, Huntley MH, Durand NC, Stamenova EK, Bochkov ID, Robinson JT, Sanborn AL, Machol I, Omer AD, Lander ES and Aiden EL. 2014. A 3d map of the human genome at kilobase resolution reveals principles of chromatin looping. *Cell* **159**(7):1665-1680. https://doi.org/10.1016/j.cell.2014.11.021.
52. Meylan S, Vimont U, Incerti S, Clairand I and Villagrasa C. 2016. Geant4-DNA simulations using complex DNA geometries generated by the DnaFabric tool. *Comput. Phys. Commun.* **204**, 159-169. https://doi.org/10.1016/j.cpc.2016.02.019.
53. Tang N, Bueno M, Meylan S, Incerti S, Tran HN, Vaurijoux A, Gruel G and Villagrasa C. 2019. Influence of chromatin compaction on simulated early radiation-induced DNA damage using Geant4- DNA. *Med. Phys.* **46**(3):1501-1511. https://doi.org/10.1002/mp.13405.
54. Takata H, Hanafusa T, Mori T, Shimura M, Iida Y, Ishikawa K, Yoshikawa K, Yoshikawa Y and Maeshima K. 2013. Chromatin compaction protects genomic dna from radiation damage. *PLOS ONE* **8**(10):e75622. https://doi.org/10.1371/journal.pone.0075622.
55. Nair N, Shoaib M and Sørensen CS. 2017. Chromatin dynamics in genome stability: Roles in suppressing endogenous dna damage and facilitating dna repair. *Int. J. Mol. Sci.* **18**(7):1486. https://doi.org/10.3390/ijms18071486.
56. Oikeh E, Ziebarth J, Dinar MAM, Kirchhoff D, Aronova A, Dziubla TD, Wang Y and DeRouchey JE. 2024. Dna packaging and polycation length determine dna susceptibility to free radical damage in condensed dna. *J. Phys. Chem. B* **128**(14):3329-3339. https://doi.org/10.1021/acs.jpcb.3c06116.
57. Ganjgah AA and Taherparvar P. 2024. The effects of cell displacement on DNA damages in targeted radiation therapy using Geant4-DNA. *Sci. Rep.* **14**(1):30015. https://doi.org/10.1038/s41598-024-81863-4.
58. Chatzipapas K, Dordevic M, Zivkovic S, Tran NH, Lampe N, Sakata D, Petrovic I, Ristic-Fira A, Shin WG, Zein S, Brown JMC, Kyriakou I, Emfietzoglou D, Guatelli S and Incerti S. 2023. Geant4-DNA simulation of human cancer cells irradiation with helium ion beams. *Phys. Med.* **112**:102613. https://doi.org/10.1016/j.ejmp.2023.102613.
59. Shin WG, Sakata D, Lampe N, Belov O, Tran NH, Petrovic I, Ristic-Fira A, Dordevic M, Bernal MA, Bordage MC, Francis Z, Kyriakou I, Perrot Y, Sasaki T, Villagrasa C, Guatelli S, Breton V, Emfietzoglou D and Incerti S. 2021. A geant4-dna evaluation of radiation-induced dna damage on a human fibroblast. *Cancers*, **13**(19):4940. https://doi.org/10.3390/cancers13194940.
60. Sakata D, Lampe N, Karamitros M, Kyriakou I, Belov O, Bernal MA, Bolst D, Bordage MC, Breton V, Brown JMC, Francis Z, Ivanchenko V, Meylan S, Murakami K, Okada S, Petrovic I, Ristic-Fira A, Santin G, Sarramia D, Incerti S. 2019. Evaluation of early radiation DNA damage in a fractal cell nucleus model using Geant4-DNA. *Phys. Med.* **62**:152-157. https://doi.org/10.1016/j.ejmp.2019.04.010.